

KELT-4Ab: AN INFLATED HOT JUPITER TRANSITING THE BRIGHT ($V \sim 10$) COMPONENT OF A HIERARCHICAL TRIPLE

JASON D. EASTMAN¹, THOMAS G. BEATTY^{2,3}, ROBERT J. SIVERD⁴, JOSEPH M. O. ANTOGNINI⁵, MATTHEW T. PENNY^{5,6}, ERICA J. GONZALES⁷, JUSTIN R. CREPP⁷, ANDREW W. HOWARD⁸, RYAN L. AVRIL⁹, ALLYSON BIERYLA¹, KAREN COLLINS¹⁰, BENJAMIN J. FULTON^{8,11}, JIAN GE¹², JOAO GREGORIO¹³, BO MA¹², SAMUEL N. MELLON^{9,14}, THOMAS E. OBERST⁹, JI WANG¹⁵, B. SCOTT GAUDI⁵, JOSHUA PEPPER¹⁶, KEIVAN G. STASSUN¹⁰, LARS A. BUCHHAVE¹, ERIC L. N. JENSEN¹⁷, DAVID W. LATHAM¹, PERRY BERLIND¹, MICHAEL L. CALKINS¹, PHILLIP A. CARGILE¹, KNICOLE D. COLÓN^{16,18,19}, SAURAV DHITAL²⁰, GILBERT A. ESQUERDO¹, JOHN ASHER JOHNSON¹, JOHN F. KIELKOPF²¹, MARK MANNER²², QINGQING MAO¹⁰, KIM K. MCLEOD²³, KALOYAN PENEV²⁴, ROBERT P. STEFANIK¹, RACHEL STREET⁴, ROBERTO ZAMBELLI²⁵, D. L. DEPOY²⁶, ANDREW GOULD⁵, JENNIFER L. MARSHALL²⁶, RICHARD W. POGGE⁵, MARK TRUEBLOOD²⁷, PATRICIA TRUEBLOOD²⁷

Draft version October 2, 2015

ABSTRACT

We report the discovery of KELT-4Ab, an inflated, transiting Hot Jupiter orbiting the brightest component of a hierarchical triple stellar system. The host star is an F star with $T_{\text{eff}}=6206 \pm 75$ K, $\log g=4.108 \pm 0.014$, $[\text{Fe}/\text{H}]=-0.116_{-0.069}^{+0.065}$, $M_*=1.201_{-0.061}^{+0.067} M_{\odot}$, and $R_*=1.603_{-0.038}^{+0.039} R_{\odot}$. The best-fit linear ephemeris is $\text{BJD}_{\text{TDB}} = 2456193.29157 \pm 0.00021 + E (2.9895936 \pm 0.0000048)$. With a magnitude of $V \sim 10$, a planetary radius of $1.699_{-0.045}^{+0.046} R_J$, and a mass of $0.902_{-0.059}^{+0.060} M_J$, it is the brightest host among the population of inflated Hot Jupiters ($R_P > 1.5R_J$), making it a valuable discovery for probing the nature of inflated planets. In addition, its existence within a hierarchical triple and its proximity to Earth (210 pc) provides a unique opportunity for dynamical studies with continued monitoring with high resolution imaging and precision radial velocities. In particular, the motion of the binary stars around each other and of both stars around the primary star relative to the measured epoch in this work should be detectable when it rises in October 2015.

Subject headings: exoplanet, transit, hot Jupiter, inflated, hierarchical triple

¹ Harvard-Smithsonian Center for Astrophysics, Cambridge, MA 02138, USA

² Department of Astronomy & Astrophysics, The Pennsylvania State University, 525 Davey Lab, University Park, PA 16802, USA

³ Center for Exoplanets and Habitable Worlds, The Pennsylvania State University, 525 Davey Lab, University Park, PA 16802, USA

⁴ Las Cumbres Observatory Global Telescope Network, Santa Barbara, CA 93117, USA

⁵ Department of Astronomy, The Ohio State University, Columbus, OH 43210, USA

⁶ Sagan Fellow

⁷ Department of Physics, University of Notre Dame, Notre Dame, IN 46556, USA

⁸ Institute for Astronomy, University of Hawaii, Honolulu, HI 96822, USA

⁹ Department of Physics, Westminster College, New Wilmington, PA 16172

¹⁰ Department of Physics and Astronomy, Vanderbilt University, Nashville, TN 37235, USA

¹¹ NSF Graduate Research Fellow

¹² Department of Astronomy, University of Florida, 211 Bryant Space Science Center, Gainesville, FL, 32611

¹³ Atalaia Group and Crow-Observatory, Portalegre, Portugal

¹⁴ Department of Physics and Astronomy, University of Rochester, Rochester, NY 14627

¹⁵ Department of Astrophysics, California Institute of Technology, MC 249-17, Pasadena, CA 91125, USA

¹⁶ Department of Physics, Lehigh University, Bethlehem, PA 18015

¹⁷ Department of Physics and Astronomy, Swarthmore College, Swarthmore, PA 19081, USA

¹⁸ NASA Ames Research Center, M/S 244-30, Moffett Field, CA 94035, USA

¹⁹ Bay Area Environmental Research Institute, 625 2nd St. Ste 209 Petaluma, CA 94952, USA

²⁰ Department of Astronomy, Boston University, 725 Commonwealth Avenue, Boston, MA 02215, USA

²¹ Department of Physics & Astronomy, University of

Louisville, Louisville, KY 40292, USA

²² Spot Observatory, Nunnely, TN 37137, USA

²³ Wellesley College, Wellesley, MA 02481, USA

²⁴ Department of Astrophysical Sciences, Princeton University, Peyton Hall, Princeton, NJ 08544, USA

²⁵ Societ Astronomica Lunae, Castelnuovo Magra 19030, Via Montefrancio, 77, Italy

²⁶ George P. and Cynthia Woods Mitchell Institute for Fundamental Physics and Astronomy, and Department of Physics and Astronomy, Texas A & M University, College Station, TX 77843-4242, USA

²⁷ Winer Observatory, Sonoita, AZ 85637, USA

1. INTRODUCTION

When Hot Jupiters were first discovered (Mayor & Queloz 1995), our understanding of planet formation and evolution was turned on its head. However, their existence made transit searches from the ground practical. Although the first transiting planets were originally discovered from follow-up of RV candidates (e.g. Charbonneau et al. 2000; Henry et al. 2000), the first detections from dedicated transit surveys followed soon after by TrES (Alonso et al. 2004), XO (McCullough et al. 2005), HAT (Bakos et al. 2002), and WASP (Collier Cameron et al. 2007), all of which had the same basic design: a small telescope with a wide field of view to monitor many stars to find the few that transited.

The Kilodegree Extremely Little Telescope (KELT) (Pepper et al. 2007) is the most extreme of the mature transit surveys, with the largest single-camera field of view (26 degrees on a side) and the largest platescale ($23''/\text{pixel}$) – similar to the planned TESS mission (Ricker et al. 2010). Therefore, while KELT is optimized to find fewer planets, it can find those around brighter host stars which allows a greater breadth and ease of follow-up to fully utilize the wealth of information the transiting planets potentially offer: planetary radius, orbital inclination (and so the true mass), stellar density (Seager & Mallén-Ornelas 2003), composition (Guillot 2005; Sato et al. 2005; Charbonneau et al. 2006; Fortney et al. 2006), spin-orbit misalignment (Queloz et al. 2000; Winn et al. 2005; Gaudi & Winn 2007; Triaud et al. 2010), atmosphere (Charbonneau et al. 2002; Vidal-Madjar et al. 2003) to name a few – see Winn (2010) for a comprehensive review.

We now describe the discovery of KELT-4Ab, an inflated Hot Jupiter ($R=1.699_{-0.045}^{+0.046} R_J$) orbiting the bright component ($V=10$) of a hierarchical triple. In terms of size, KELT-4Ab is qualitatively similar to WASP-79b (Smalley et al. 2012) and WASP-94Ab (Neveu-VanMalle et al. 2014), which have slightly larger planets around slightly fainter stars. Its size is also similar to KELT-8b (Fulton et al. 2015). See section 6.2 of Fulton et al. (2015) for a more detailed comparison of similar planets. KELT-4Ab is only the third known transiting planet in a hierarchical triple stellar system, along with WASP-12b and HAT-P-8b (Bechter et al. 2014). KELT-4 is the brightest host of all these systems, and therefore a valuable find for extensive follow-up of both inflated planets and hierarchical architectures. Because it is relatively nearby (210 pc), continued AO imaging will be able to provide dynamical constraints on the stellar system.

2. DISCOVERY AND FOLLOW-UP OBSERVATIONS

The procedure we used to identify KELT-4Ab is identical to that described in Siverd et al. (2012), using the setup described in Pepper et al. (2007), both of which we summarize briefly here.

KELT-4Ab was discovered in field 06 of our survey, which is a $26^\circ \times 26^\circ$ field of view centered at J2000 09:46:24.1, +31:39:56, best observed in February. We took 150 second exposures with our 42 mm telescope lo-

cated at Winer Observatory²⁸ in Sonoita, Arizona, with a typical cadence of 15-30 minutes as we cycled between observable fields.

Each object in the KELT survey is matched to the Tycho-2 (Høg et al. 2000) and 2MASS (Cutri et al. 2003; Skrutskie et al. 2006) catalogs, which we use to derive a reduced proper motion cut to remove giants from our sample (Collier Cameron et al. 2007). After image subtraction, outliers are clipped and the light curves are detrended with the Trend Filtering Algorithm (Kovács et al. 2005), and a BLS search is performed (Kovács et al. 2002). After passing various programmatic cuts described in Siverd et al. (2012), candidates are inspected by eye and selected for follow-up. Figure 1 shows the KELT discovery light curve for KELT-4Ab.

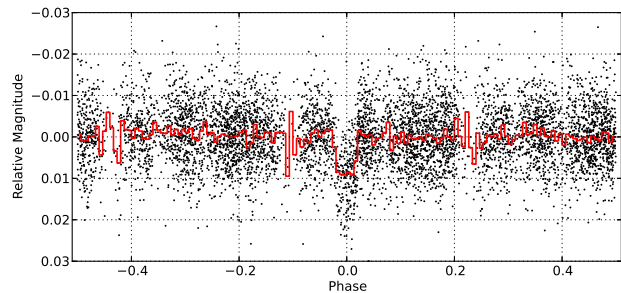


FIG. 1.— The TFA-detrended discovery light curve for KELT-4Ab showing all 6571 data points KELT collected from 2006-10-27 to 2011-04-01 (when it was flagged for radial velocity follow-up), phase folded at the best BLS period of 2.9895365 days. The red line shows the data binned in 150 bins (~ 29 minutes).

2.1. SuperWASP

As part of the by-eye object selection, we inspect the corresponding public SuperWASP data, if available (Butters et al. 2010). While SuperWASP achieved roughly the same photometric precision with almost as many observations as KELT did, due to the near-integer period of KELT-4Ab (Period = 2.9895936 ± 0.0000048) and the relatively short span of the SuperWASP observations, SuperWASP did not observe the ingress of the planet, as shown in Figure 2.

While HAT and SuperWASP adopt a strategy to change fields often, likely because of the shallow dependence of the detectability with the duration of observations (Beatty & Gaudi 2008), KELT has generally opted to monitor the same fields for much longer, increasing its sensitivity to longer and near-integer periods, as demonstrated by this find.

2.2. Follow-up photometry

We have amassed an extensive follow-up network consisting of around 30 telescopes from amateurs, universities, and professional observatories. Coordinating with the KELT team, collaborators obtained 19 high-quality transits in six bands with six different telescopes, shown in Figure 3. All transits are combined and binned in 5-minute intervals in Figure 4 to demonstrate the statistical power of the combined fit to the entire dataset,

²⁸ <http://winer.org/>

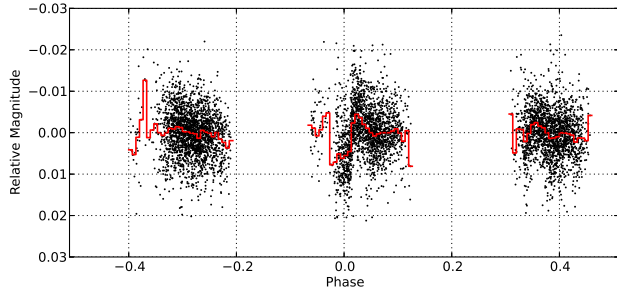


FIG. 2.— The observations from two good seasons and cameras of public SuperWASP data for KELT-4Ab (Butters et al. 2010), showing 6020 points from 2006-04-01 to 2007-05-05, phase folded at the KELT BLS period of 2.9895365 days. The red line shows the data binned in 150 bins (~ 29 minutes). Despite observing the star at roughly the same precision and obtaining nearly as many data points as KELT, the near-integer period of KELT-4Ab and relatively short span of observations makes SuperWASP’s phase coverage sparse, which explains why SuperWASP was not able to identify KELT-4Ab in their data.

as well as the level of systematics present in this combined fit, though this combined light curve was not used directly for analysis.

We used KeplerCam on the 1.2 meter Fred Lawrence Whipple Observatory (FLWO) telescope at Mount Hopkins to observe ten transits of KELT-4Ab in the Sloan i , g , and z bands. These are labeled “FLWO” in Figure 3. In the end, only eight of these transits were used in the final fit. We excluded one transit on the night of UT 2013-01-15. Cloudy weather forced the dome to close twice during the first half of the observations. Thin clouds continued throughout egress. When analyzed, these data produced a 7σ significant outlier in the transit time, hinting at large systematics in this lightcurve. We include it with our electronic tables for completeness, but due to the cloudy weather, we do not include it in our analysis. We also excluded another transit observed on the night of UT 2012-05-11. While there is no obvious fault with the light curve, our MCMC analysis found two widely separated, comparably likely regions of parameter space by exploiting a degeneracy in the baseline flux and the airmass detrending parameter, which significantly degraded the quality of the global analysis. Again, we include this observation in the electronic tables for completeness, but do not use it for our analysis. The change in the best-fit parameters of KELT-4Ab is negligible whether this transit is included or not.

We observed four transits, two in the Sloan g , one in Sloan r , and one in Sloan i , at the Moore Observatory using the 0.6m RCOS telescope, operated by the University of Louisville in Kentucky (labeled “ULMO”) and reduced with the AstroImageJ package (Collins & Kielkopf 2013; Collins 2015). See Collins et al. (2014) for additional observatory information.

We observed two transits at the Westminster College Observatory in Pennsylvania (labeled “WCO”) with a Celestron C14 telescope in the CBB (blue blocking) filter. As there are no limb darkening tables for this filter in Claret & Bloemen (2011), we modeled it as the closest analog available – the CONvection ROTation and planetary Transits (CoRoT) bandpass (Baglin et al. 2006).

Las Cumbres Observatory Global Telescope (LCOGT) consists of a 0.8 meter prototype telescope and nine 1-

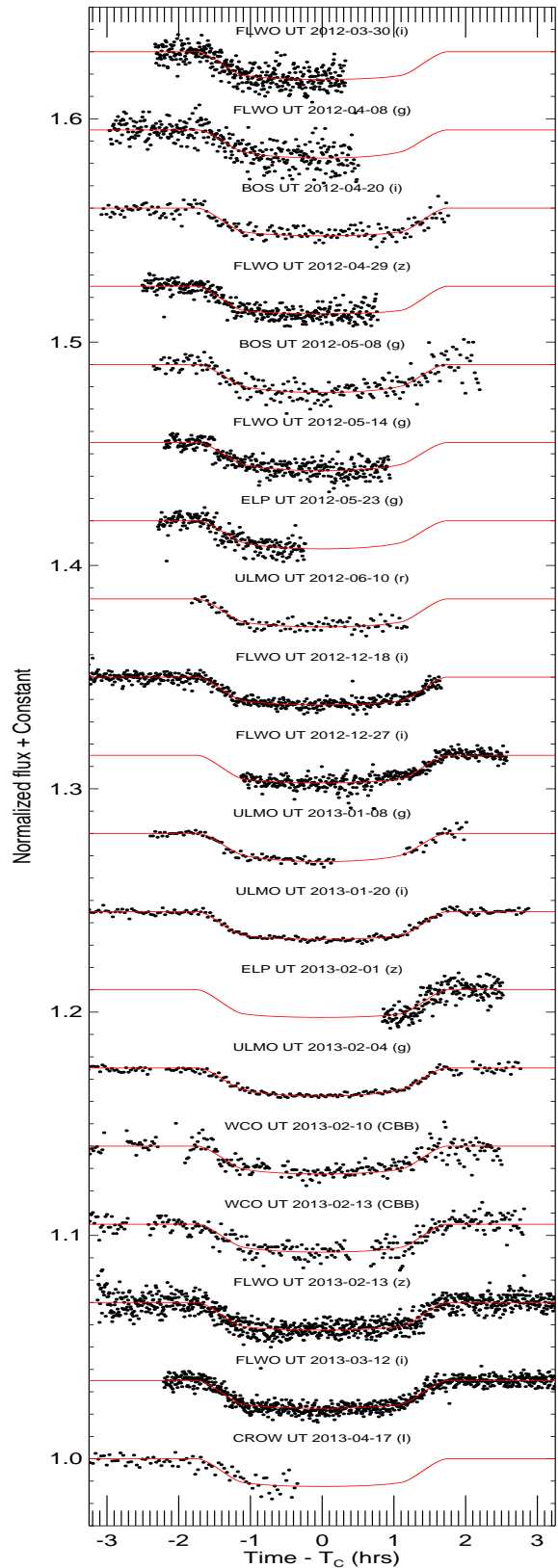


FIG. 3.— The 19 follow-up light curves analyzed for KELT-4Ab, in black, with the best-fit model (see §3) shown in red. Each light curve has had the SED-modeled contamination from the stellar companion subtracted, the out of transit flux normalized to unity and offset by an arbitrary constant for clarity, the best fit transit time, T_C subtracted, and a trend with airmass removed. The labels above each light curve display the telescope, UT date, and filter corresponding to each observation.

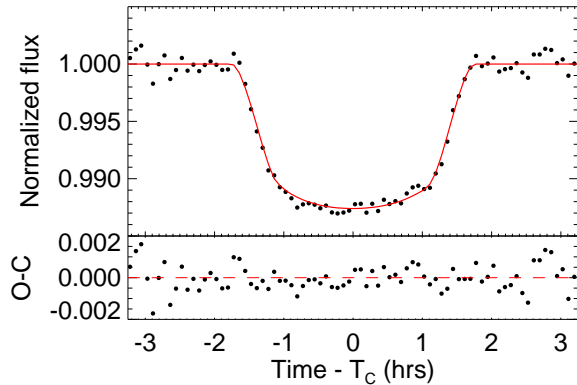


FIG. 4.— (Top panel) The 19 follow-up light curves for KELT-4Ab, binned in 5-minute intervals. This is not used during analysis, but is just to show the statistical power of the combined fit to the entire dataset, as well as the level of systematics present in this combined fit. Overlaid is the model for each of the 19 light curves averaged in the same way. (Bottom panel) The residuals of the binned light curve from the binned model in the top panel.

meter telescopes spread around the world (Brown et al. 2013). We used the prototype telescope (labeled “BOS”) to observe transits in the Sloan i band and the Sloan g band. Additionally, we used the 1 meter telescope at McDonald Observatory in Texas (labeled “ELP”) to observe two partial transits in the Sloan g band and Pan Starrs z band. As there are no limb darkening tables for Pan-Starrs z in Claret & Bloemen (2011), we modeled it as the closest analog available – the Sloan z filter.

We observed one partial transit in the I band at Canela’s Robotic Observatory (labeled “CROW”) in Portugal on UT 2013-04-17. The observations were obtained using a 0.3m LX200 telescope with an SBIG ST-8XME 1530x1020 CCD, giving a 28’x 19’ field of view and 1.11 arcseconds per pixel.

2.3. Radial Velocity

We obtained Radial Velocity (RV) measurements of KELT-4A from three different telescopes/instruments, shown in Figures 5 and 6, and summarized in Table 1. The table expresses the radial velocities as relative velocities, using the raw velocities and subtracting the best-fit instrumental velocities from each. For the HIRES velocities, absolute RVs were measured with respect to the telluric lines separately, using the method described by Chubak et al. (2012) with a mean offset of $-23.5 \pm 0.1 \text{ km s}^{-1}$.

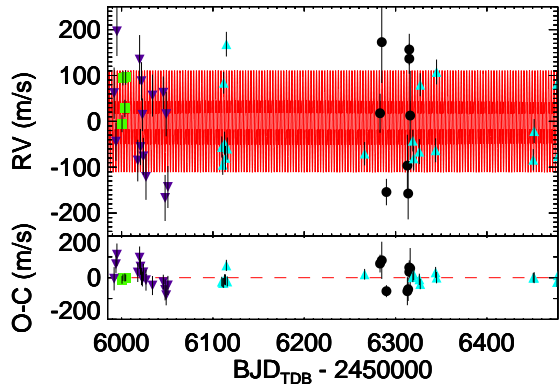


FIG. 5.— (Top panel) The unphased RVs for KELT-4A showing HIRES (blue upward triangles), FIES (green squares), EXPERT (black circles), and TRES (purple downward triangles) and the best-fit model in red. The systemic velocity of -23.5 km s^{-1} has been subtracted for clarity. (Bottom panel) The residuals of the RV data from the model fit.

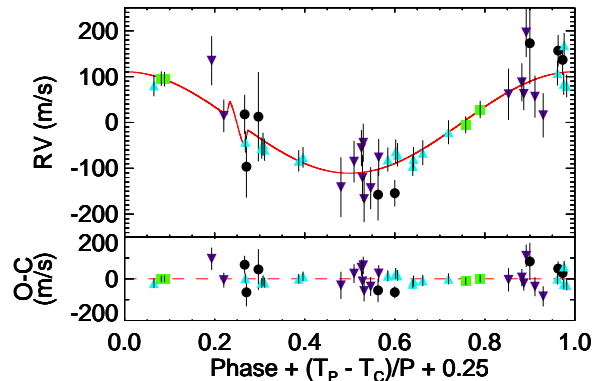


FIG. 6.— (Top panel) The phased RV curve for KELT-4Ab showing HIRES (blue upward triangles), FIES (green squares), EXPERT (black circles), and TRES (purple downward triangles). The best-fit model is shown in red, including the Rossiter-McLaughlin (RM) effect. Note that the spin-orbit alignment is extremely poorly constrained by the three points in three different transits and does not conclusively exclude any value. The units of the x-axis were chosen such that the time of transit is centered at 0.25. (Bottom panel) The residuals of the RV data from the model fit.

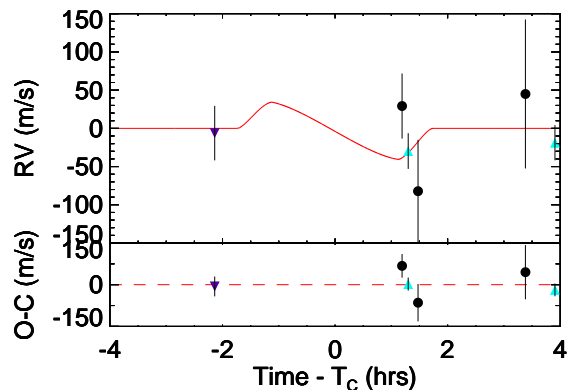


FIG. 7.— (Top panel) The phased Rossiter-McLaughlin effect for KELT-4A with the planetary radial velocity signal subtracted showing the one HIRES point and two EXPERT points taken in transit, as well as a few other data points near transit, with the same legend as figures 5 and 6. The best-fit model is shown in red, using the Ohta et al. (2005) model. Note that the spin-orbit alignment is extremely poorly constrained by the three points in three different transits and does not conclusively exclude any value. (Bottom panel) The residuals of the RV data from the best-fit model.

TABLE 1
RV OBSERVATIONS OF KELT-4A

BJD (TDB)	RV ^a (m s ⁻¹)	RV error ^b (m s ⁻¹)	Source
2455984.708730	-144.39	31.28	TRES
2455991.800887	58.13	26.81	TRES
2455993.825798	-47.76	19.93	TRES
2455994.907665	192.71	25.75	TRES
2456000.485110	-0.50	18.50	FIES
2456001.474912	99.00	15.90	FIES
2456003.570752	32.70	18.80	FIES
2456004.443338	100.20	15.90	FIES
2456017.681414	-89.66	21.74	TRES
2456019.725231	130.45	25.66	TRES
2456020.719807	-60.29	18.91	TRES
2456021.785077	83.22	19.91	TRES
2456022.795489	10.00	17.07	TRES
2456023.824122	-80.68	19.33	TRES
2456026.706127	-125.61	23.94	TRES
2456033.830514	51.58	21.88	TRES
2456045.714834	57.37	17.07	TRES
2456047.644014	-172.04	24.07	TRES
2456048.833086	10.57	23.13	TRES
2456050.677247	-148.27	21.92	TRES
2456109.745582	-48.13	3.36	HIRES
2456110.748739	-86.97	3.19	HIRES
2456111.750845	91.86	3.46	HIRES
2456112.744005	-39.81	3.66	HIRES
2456113.743451	-71.90	3.80	HIRES
2456114.743430	176.00	3.92	HIRES
2456115.743838	-51.79	3.54	HIRES
2456266.106636	-67.17	3.72	HIRES
2456283.028749	18.00	31.00	EXPERT ^c
2456284.922216	173.00	65.00	EXPERT
2456290.004820	-154.00	21.00	EXPERT
2456312.936489	-97.00	49.00	EXPERT ^c
2456313.810429	-158.00	41.00	EXPERT
2456315.006329	156.00	25.00	EXPERT
2456315.035867	136.00	24.00	EXPERT
2456316.005608	12.00	71.00	EXPERT
2456318.908411	-40.54	3.41	HIRES ^c
2456319.854373	-79.04	3.83	HIRES
2456326.065752	-64.53	3.96	HIRES
2456327.021240	81.25	3.64	HIRES
2456343.823502	-62.11	3.80	HIRES
2456344.897907	108.59	3.96	HIRES
2456450.804949	-85.90	3.39	HIRES
2456451.799327	-23.46	3.83	HIRES
2456476.749960	77.81	3.46	HIRES
2456477.739810	-79.00	3.29	HIRES

^a The offsets for each telescope have been fitted and subtracted. The systemic velocity, measured from Keck as -23.5 ± 0.1 km s⁻¹ may be added to each observation to get the absolute velocities.

^b Unscaled measurement uncertainties.

^c Observation occurred during transit and was affected by the Rossiter-McLaughlin effect.

Using the High Resolution Echelle Spectrometer (HIRES) instrument (Vogt et al. 1994) on the Keck I telescope located on Mauna Kea, Hawaii, we obtained 16 exposures between 2012-07-01 and 2013-02-21 with

an iodine cell, plus a single iodine-free template spectrum. One of these points fell within the transit window and therefore provides a weak constraint on the Rossiter-McLaughlin effect (see Figure 7). We followed standard procedures of the California Planet Survey (CPS) to set up and use HIRES, reduce the spectra, and compute relative RVs (Howard et al. 2010). We used the ‘‘C2’’ decker (0.86’’ wide) and oriented the slit with an image rotator to avoid contamination from KELT-4B,C.

We obtained five spectra with the Fibre-fed Echelle Spectrograph (FIES) on the 2.5 meter Nordic Optical Telescope (NOT) in La Palma, Spain (Djupvik & Andersen 2010) between 2012-03-13 and 2012-03-17 with the high-resolution fiber (1.3’’ projected diameter) with resolving power $R \approx 67,000$. We discarded one observation which the observer marked as bad and had large quoted uncertainties. We used standard procedures to reduce these data, as described in Buchhave et al. (2010) and Buchhave et al. (2012).

Eight spectra were taken with the EXPERT spectrograph (Ge et al. 2010) at the 2.1m telescope at Kitt Peak National Observatory between 2012-12-21 and 2013-01-23 and reduced using a modified pipeline described by Wang et al. (2012). EXPERT has a resolution of $R=30,000$, 0.39-1.0 μm coverage, and a 1.2’’ fiber. Two of these spectra were taken during transit and therefore provide a weak constraint on the RM effect.

We took 16 radial velocity observations with the TRES spectrograph (Fűrész 2008), which has a resolving power of 44,000, a fiber diameter of 2.3’’, and a typical seeing of 1.5’’. Because of the typical seeing, the fiber diameter, and the nearby companion, we initially excluded all of the TRES data, but when we found the fit to be consistent (albeit with slightly higher scatter than is typical for TRES), we included it in the global fit. The higher scatter was taken into account by scaling the errors such that the probability of χ^2 we got was 0.5, as we do for all data sets.

Stellar parameters ($\log g$, T_{eff} , $[\text{Fe}/\text{H}]$, and $v \sin I_*$) were derived from the FIES and TRES using the Stellar Parameter Classification (SPC) tool (Buchhave et al. 2014), and the HIRES spectra using SpecMatch (Pettigura et al. 2015 in prep.). It is well known that the transit lightcurve alone can constrain the stellar density (Seager & Mallén-Ornelas 2003). Coupled with the YY isochrones and a measured T_{eff} , the transit light curve provides a tight constraint on the $\log g$ (Torres et al. 2012). Alternatively, we have discovered that the limb darkening of the transit itself is sufficient to loosely constrain the T_{eff} and therefore the $\log g$ without spectroscopy during a global fit, which we use as another check on the stellar parameters. Finally, we iterated on the HIRES spectroscopic parameters using a prior on the $\log g$ from the global fit. That is, we used the HIRES spectroscopic parameters to seed a global fit, found the $\log g$ using the more precise transit constraint, fed that back into SpecMatch to derive new stellar parameters that are consistent with the transit, and then ran the final global fit.

All of these methods were marginally consistent ($< 1.7\sigma$) with one another, as shown in Table 2. Since the uncertainties in the measured stellar parameters are typically dominated by the stellar atmospheric models, this marginal consistency is uncommon and may be indica-

tive of a larger than usual systematic error. It is likely that the discrepancy is due to the blend with the neighbor 1.5’’ away. While the FIES $\log g$ agrees best with the $\log g$ derived from the transit photometry, we adopted the HIRES parameters derived with an iterative $\log g$ prior from the global analysis because of its higher spatial resolution and better median site seeing. However, to account for the inconsistency between methods, we inflated the uncertainties in T_{eff} and $[\text{Fe}/\text{H}]$ as shown in Table 2 so they were in good agreement with the values without the $\log g$ prior and did not include a spectroscopic prior on the $\log g$ during the global fit. Still, systematic errors in the stellar parameters (and therefore the derived planetary parameters) at the 1-sigma level would not be surprising. The slightly hotter star preferred by the other spectroscopic methods would make the star bigger and therefore the planet even more inflated. The cooler star preferred by the limb darkening would make the star and planet smaller.

2.4. Historical Data

As compiled by the Washington Double Star Catalog (Mason et al. 2001), KELT-4 was originally identified as a common proper motion binary with a separation of 1.5’’ by Couteau (1973), who named it COU 777. It was later observed in 1987 by Argue et al. (1992), *Hipparcos* in 1991 (Perryman et al. 1997; van Leeuwen 2007), and the Tycho Survey in 1991 (Fabricius et al. 2002). The magnitudes, position angles (degrees East of North), and separations (arcseconds) from these historical records are summarized in Table 3 at the observed epochs, in addition to our own measurement described in §2.5.

2.5. High-Resolution Imaging

On 2012-05-07, we obtained adaptive optics (AO) imaging on the Keck II telescope located on Mauna Kea, Hawaii, using NIRC2 in both the J and K bands (Yelda et al. 2010), shown in Figure 8. We used the narrow camera, with a pixel scale of 0.009942’’/pix.

The proper motion determined by *Hipparcos* of $\mu_\alpha = 11.79 \pm 1.31 \text{ mas yr}^{-1}$ and $\mu_\delta = -12.63 \pm 0.9 \text{ mas yr}^{-1}$ over the 40-year baseline between the original observations by Couteau (1973) and ours have amounted to over 0.5’’ of total motion. If the companion mentioned in §2.4 was not gravitationally bound, this motion would have significantly changed the separation, which would be trivial to detect in our AO images. However, the separations remain nearly identical. Therefore, we confirm this system as a common proper motion binary.

Interestingly, for the first time, our AO image further resolves the stellar companion as a binary itself, with a separation of $49.14 \pm 0.39 \text{ mas}$ and a position angle of $325.23 \pm 0.13 \text{ degrees}$ at epoch 2012.3464, as shown in Figure 8. From their relative magnitudes and SED modeling, we estimate this pair to be twin K stars with $T_{\text{eff}} = 4300 \text{ K}$ and $R_* = 0.6 \pm 0.1 R_\odot$. Using Demory et al. (2009), we translate that to a mass of $0.65 \pm 0.1 M_\odot$. Therefore, KELT-4Ab is a companion to the brightest member of a hierarchical triple stellar system, similar to WASP-12b and HAT-P-8b (Bechter et al. 2014). That is, KELT-4A is orbited by KELT-4Ab, a $\sim 1M_J$ mass planet with a period of 3 days and also by KELT-4BC, a twin K-star binary. In all of our follow-up

TABLE 2
SUMMARY OF MEASURED STELLAR PARAMETERS

Instrument	$\log g$ cgs	T_{eff} K	[Fe/H]	$v \sin I_*$ km s ⁻¹
FIES	4.11 ± 0.10	6360 ± 49	-0.12 ± 0.08	7.6 ± 0.5
TRES	4.05 ± 0.10	6249 ± 49	-0.12 ± 0.08	7.8 ± 0.5
HIRES	4.20 ± 0.08	6281 ± 70	-0.10 ± 0.05	7.6 ± 1.7
HIRES ^a	4.12 ± 0.08	6218 ± 70	-0.12 ± 0.05	6.2 ± 1.2
Global fit ^b	4.104 ± 0.019	6090^{+390}_{-320}	—	—
Adopted priors ^c	N/A	6218 ± 80	-0.12 ± 0.08	6.2 ± 1.2
Final values ^d	4.108 ± 0.014	6206 ± 75	$-0.116^{+0.065}_{-0.069}$	6.2 ± 1.2

^a Includes an iterative $\log g$ prior from the global transit fit.

^b Values from the global fit without a $\log g$ or T_{eff} prior, but with an [Fe/H] = -0.12 ± 0.08 prior and guided by the stellar limb darkening.

^c Spectroscopic priors used in the final iteration of the global fit.

^d The values from the final iteration of the global fit with the adopted spectroscopic priors.

TABLE 3
THE POSITIONS OF THE COMPONENTS OF KELT-4 FROM HISTORICAL DATA.

Epoch	$PA_{A,BC}$ (degrees)	$Sep_{A,BC}$ (arcsec)	PA_{BC} (degrees)	Sep_{BC} (mas)	V_A	V_{BC}	R_A	R_{BC}	J_A	J_{BC}	K_A	K_{BC}	Source
1972.230	38.9	1.430	—	—	9.500	14.000	—	—	—	—	—	—	1
1972.249	34.0	1.570	—	—	9.500	14.000	—	—	—	—	—	—	1
1987.430	35.0	1.380	—	—	10.130	12.370	9.81	11.96	—	—	—	—	2
1991.250	31.0	1.553(43)	—	—	10.186	12.992	—	—	—	—	—	—	3
1991.530	33.1	1.560	—	—	10.042	12.992	—	—	—	—	—	—	4
2012.3464	28.887(70)	1.5732(18)	325.23(13)	49.14(39)	—	—	—	—	9.193	10.94	8.972	10.35	5

REFERENCES. — 1=Couteau (1973); 2=Argue et al. (1992); 3=Perryman et al. (1997); van Leeuwen (2007); 4=Fabricius et al. (2002); 5=This work

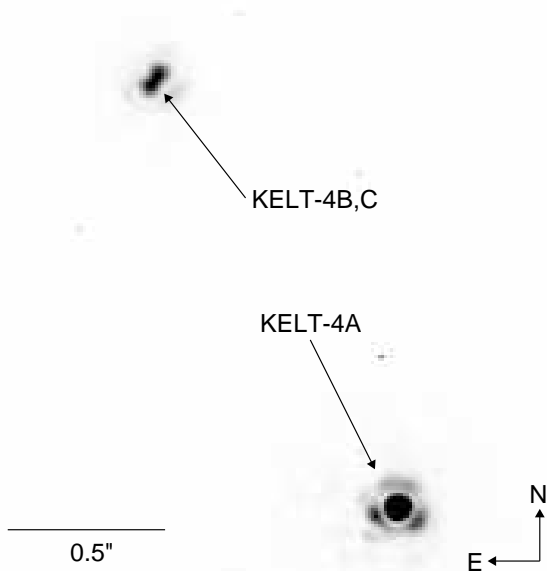


FIG. 8.— The KECK AO image taken by the NIRC2 instrument in the K band shows KELT-4A in the bottom right, and a physically-bound, blended binary star (KELT-4B,C) 1.5" to the northeast.

At the distance of 210 pc determined from our SED modeling (§3.1), the projected separation between KELT-4A and KELT-4BC is 328 ± 16 AU, and the projected separation KELT-4B and KELT-4C is 10.3 ± 0.74 AU. Assuming the orbit is face on and circular, the period of the outer binary, $P_{A,BC}$, would be 3780 ± 290 years and the period of the twin stars, $P_{B,C}$, would be 29.4 ± 3.6 years.

While assuming the orbit is face on and circular is likely incorrect, it gives us a rough order of magnitude of the signal we might expect. If correct, in the 21 years between *Hipparcos* and Keck data, we would expect to see about 55 mas of motion of KELT-4BC relative to KELT-4A. This is roughly what we see, though it is worth noting that the clockwise trend between the *Hipparcos* position and our measurement is in contradiction to the 1-sigma counter-clockwise trend for the two *Hipparcos* values.

Extending the baseline to the full 40 years, we expect to see about 110 mas of motion. While the historical values are quoted without uncertainties, using the 200 mas discrepancy between the two 1972 data points as a guide, the data seem to confirm the clockwise trend and are consistent with a 110 mas magnitude (see Figure 9). Unfortunately, the data sample far too little of the orbit and are far too imprecise to provide meaningful constraints on any other orbital parameters.

light curves, this double, with a combined V magnitude of 13, was blended with KELT-4, contributing $\sim 2 - 7\%$ to the baseline flux, depending on the observed bandpass.

3. MODELING

3.1. SED

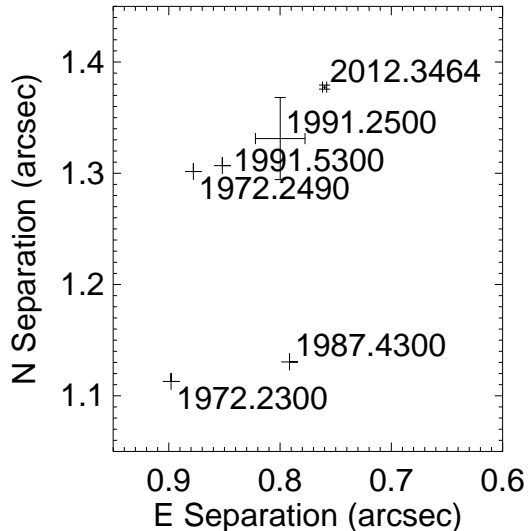


FIG. 9.— The positions of KELT-4BC relative to KELT-4A from Table 3. The epochs of each observation are printed next to the corresponding data point, showing the slow clockwise motion. Note that the data point from this work has error bars smaller than the point, and several points do not have quoted uncertainties.

We used the broadband photometry for the combined light for all three components, summarized in Table 4, the spectroscopic value of T_{eff} , and an iterative solution for R_* from EXOFAST to model the SED of KELT-4A and KELT-4BC, assuming the B and C components were twins.

The SED of KELT-4 is shown in Figure 10, using the blended photometry from all 3 components summarized in Table 4. We fit for extinction, A_V and the distance, d . A_V was limited to a maximum of 0.05 based on the Schlegel dust map value (Schlegel et al. 1998) for the full extinction through the Galaxy along the line of sight). From the SED analysis, we derive an extinction of 0.01 mag and a distance of 210 ± 10 pc – consistent with, but much more precise than the *Hipparcos* parallax (330 ± 150 pc).

Because KELT-4A was blended with KELT-4BC in all of our transit photometry, the SED-modeled contributions from KELT-4B and KELT-4C were subtracted before modeling the transit. The contribution from the KELT-4BC component was 1.827% in Sloan g , 4.077% in Sloan r , 5.569% in Sloan i , 7.017% in Sloan z , and 3.670% in *CBB*.

We ran several iterations of the EXOFAST fit (see §3.3), first with a prior on the distance from the SED modeling, but without priors on T_{eff} or $\log g$. The R_* from EXOFAST was fed back into the SED model, and we iterated until both methods produced consistent values for T_{eff} and $\log g$.

Because the distance derived from the SED modeling relies on the R_* from EXOFAST, we removed the distance prior during the final iteration of the global fit so as not to double count the constraint. The only part of the SED modeling our global fit relies on is the extinction and the blending fractions in each bandpass that dilute the transit depth. The details of the iterative fit

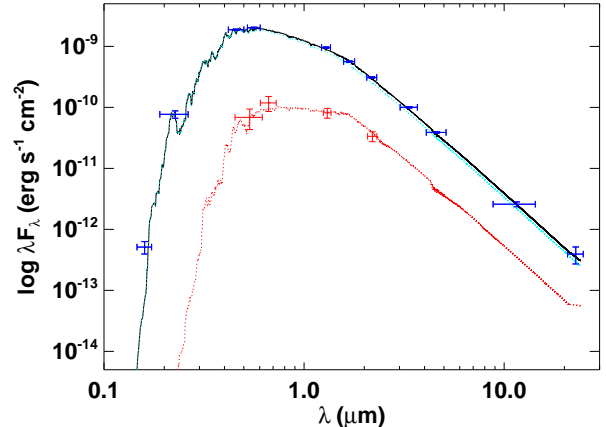


FIG. 10.— Measured and best-fit SEDs for KELT-4A (cyan), the combined SED from KELT-4B and KELT-4C (red) and the combined light from KELT-4A, KELT-4B, and KELT-4C (black) from UV through NIR. The error bars indicate measurements of the flux in UV, optical, and NIR passbands listed in Tables 4 and 3. The vertical errorbars are the 1σ photometric uncertainties, whereas the horizontal error bars are the effective widths of the passbands. The solid curves are the best-fit theoretical SED from the NextGen models of Hauschildt et al. (1999), assuming stellar parameters T_{eff} , $\log g$, and $[\text{Fe}/\text{H}]$ fixed at the values in Table 4 from the circular fit, with A_V and d allowed to vary.

are described further in §3.3.

3.2. Galactic Model

Using the distance, proper motion, the systemic velocity from Keck, and the Coşkunoglu et al. (2011) determination of the Sun’s peculiar motion with respect to the local standard of rest, we calculate the 3-space motion of the KELT-4A system through the Galaxy, summarized in table 4. According to the classification scheme of Bensby et al. (2003), this gives the system a 99% likelihood of being in the Galaxy’s thin disk, which is consistent with the other known parameters of the system.

3.3. Global Model

Similar to Beatty et al. (2012), after iterative SED modeling and transit modeling with the blend subtracted converged on the same stellar properties, we used a modified version of EXOFAST (Eastman et al. 2013) to model the unblended KELT-4A parameters, radial velocities, and debledned transits in a global solution.

We imposed Gaussian priors for $T_{\text{eff}} = 6218 \pm 80$ K, $[\text{Fe}/\text{H}] = -0.12 \pm 0.08$, and $V \sin I_* = 6.2 \pm 1.2$ km s $^{-1}$ from the Keck high resolution spectra as measured by SpecMatch with an iterative solution on $\log g$ from the global fit. The uncertainties in $[\text{Fe}/\text{H}]$ and T_{eff} were inflated due to the marginal disagreement with the parameters measured by FIES and TRES, as discussed in §2.3.

We also imposed Gaussian priors from a linear fit to the transit times: $P = 2.9895933 \pm 0.0000049$ and $T_C = 2456190.30201 \pm 0.00022$. These priors do not affect the measured transit times since a separate TTV was fit to each transit without limit. These priors only impact the RV fit, the timing of the RM effect, and the shape of the transit slightly through the period. In addition, we fixed the extinction, A_V to 0.01 and the debrending fractions

TABLE 4
 STELLAR PROPERTIES OF KELT-4A AND COMBINED PHOTOMETRY FOR ALL THREE COMPONENTS USED FOR THE SED FIT.

Parameter	Description (Units)	Value	Source	Reference
Names		BD+26 2091 HIP 51260 GSC 01973-00954 SAO 81366 2MASS J10281500+2534236 TYC 1973 954 1 CCDM J10283+2534A WDS 10283+2534 GALEX J102814.9+253423 COU 777		
α_{J2000}	Right Ascension (J2000)	10 28 15.011	Hipparcos	1
δ_{J2000}	Declination (J2000)	+25 34 23.47	Hipparcos	1
FUV_{GALEX}	Far UV Magnitude	20.39 ± 0.16	GALEX	2
NUV_{GALEX}	Near UV Magnitude	14.49 ± 0.01	GALEX	2
B	Johnson B Magnitude	10.47 ± 0.03	APASS	3
V	Johnson V Magnitude	9.98 ± 0.03	APASS	3
J	J Magnitude	9.017 ± 0.021	2MASS	4
H	H Magnitude	8.790 ± 0.023	2MASS	4
K	K Magnitude	8.689 ± 0.020	2MASS	4
WISE1	WISE 3.6 μm	8.593 ± 0.022	WISE	5
WISE2	WISE 4.6 μm	8.642 ± 0.020	WISE	5
WISE3	WISE 11 μm	8.661 ± 0.023	WISE	5
WISE4	WISE 22 μm	8.608 ± 0.336	WISE	5
μ_α	Proper Motion in RA (mas yr ⁻¹)	11.79 ± 1.31	Hipparcos	1
μ_δ	Proper Motion in Dec (mas yr ⁻¹)	-12.63 ± 0.90	Hipparcos	1
π^a	Parallax (mas)	3.02 ± 1.41	Hipparcos	1
d^a	Distance (pc)	211^{+13}_{-12}	This work (Eccentric)	
d^a	Distance (pc)	210.7 ± 9.0	This work (Circular)	
d^a	Distance (pc)	210 ± 10	This work (SED)	
U^b	Galactic motion (km s ⁻¹)	33.2 ± 1.3	This work	
V	Galactic motion (km s ⁻¹)	9.8 ± 1.0	This work	
W	Galactic motion (km s ⁻¹)	-8.6 ± 0.7	This work	
A_V	Visual Extinction	$0.05^{+0.0}_{-0.03}$	This work	

REFERENCES. — 1=Perryman et al. (1997); van Leeuwen (2007); 2=Martin et al. (2005); 3=Henden et al. (2012); 4=Cutri et al. (2003); Skrutskie et al. (2006); 5=Wright et al. (2010); Cutri & et al. (2012);

^a We quote the parallax from Hipparcos, but derive a more precise distance from our SED modeling and semi-independently through both the eccentric and circular global EXOFAST models. While all are consistent, we adopt the SED distance as our preferred value.

^b Positive U is in the direction of the Galactic Center.

for each band summarized in §3.1 from the SED analysis, and the V-band magnitude to 10.042 from Tycho in order to derive the distance.

The errors for each data set were scaled such that the probability of obtaining the χ^2 we got from an independent fit was 0.5. For all the transit data, the scaled errors are reported in the online data sets. For the eccentric fit to the EXPERT data, which did not have enough data points for an independent fit, we iteratively found the residuals from the global fit and scaled the uncertainties based on that. The FIES data, with only four good data points, also did not have enough data points for independent fits for either the eccentric or circular fits. However, it had a scatter about the best-fit global model that was smaller than expected. We opted not to scale the FIES uncertainties at all, as enforcing a $\chi_\nu^2 = 1$ would result in uncertainties that were significantly smaller than HIRES, which is not justified based on our experience with both instruments. The scalings for each fit and RV data set are reported in Table 6. Note that a common jitter term for all data sets does not reproduce a $\chi_\nu^2 = 1$ for each data set, as one would expect if the stellar jitter were the sole cause of the additional scatter. We would require a 55 m s^{-1} jitter term for the EXPERT and TRES

data sets and a 23 m s^{-1} jitter term for the HIRES RVs. The FIES χ_ν^2 is below 1, so no jitter term could compensate. We suppose that contamination is to blame for the higher scatter in the TRES and EXPERT data, while the limited number of data points makes it relatively likely to get a smaller-than-expected scatter by chance for the FIES data.

We replaced the Torres relation within EXOFAST with Yonsie Yale (YY) evolutionary tracks (Yi et al. 2001; Demarque et al. 2004) to derive the stellar properties more consistently with the SED analysis. At each step in the Markov chain, R_* was derived from the step parameters. That, along with the steps in $\log M_*$ and $[\text{Fe}/\text{H}]$ were used as inputs to the YY evolutionary tracks to derive a value for T_{eff} . Since there are sometimes more than one value of T_{eff} for given values of $\log M_*$ and $[\text{Fe}/\text{H}]$, we use the YY T_{eff} closest to the step value for T_{eff} . The global model is penalized by the difference between the YY-derived T_{eff} and the MCMC step value for T_{eff} , assuming a YY model uncertainty of 50 K, effectively imposing a prior that the host star lie along the YY evolutionary tracks. The step in T_{eff} was further penalized by the difference between it and spectroscopic prior in T_{eff} to impose the spectroscopic constraint. This same

method was used in all KELT discoveries including and after KELT-6b, as well as HD 97658b (Dragomir et al. 2013).

The distance derived in Table 6 does not come from an explicit prior from the SED analysis. Rather, the value quoted in the table is derived through the transit $\log g$ and the $[\text{Fe}/\text{H}]$ and T_{eff} priors coupled with the YY evolutionary tracks (i.e., the stellar luminosity), the extinction, the magnitude, and the bolometric correction from Flower (1996) (and $M_{\text{bol},\odot} = 4.732$, Torres et al. (2010)). The agreement in the distances derived from EXOFAST and the SED analysis is therefore a confirmation that the two analyses were done self-consistently. We adopt the distance determination from the SED fit (210 ± 10 pc) as the preferred value.

The quadratic limb darkening parameters, summarized in Table 5, were derived by interpolating the Claret & Bloemen (2011) tables with each new step in $\log g$, T_{eff} , and $[\text{Fe}/\text{H}]$ and not explicitly fit. Since this method ignores the systematic model uncertainty in the limb darkening tables, which likely dominate the true uncertainty, we do not quote the MCMC uncertainties. All light curves observed in the same filter used the same limb darkening parameters.

We modeled the system allowing a non-zero eccentricity of KELT-4Ab, but found it perfectly consistent with a circular orbit. This is generally expected because the tidal circularization timescales of such Hot Jupiters are much much smaller than the age of the system (Adams & Laughlin 2006). Therefore, we reran the analysis fixing KELT-4Ab’s eccentricity to zero. The results of both the circular and eccentric global analyses are summarized in Table 6, though we generally favor the circular fit due to our expectation that the planet is tidally circularized and the smaller uncertainties. All figures and numbers shown outside of this table are derived from the circular fit.

While we only had 3 serendipitous radial velocity data points during transit, we allowed λ , the spin-orbit alignment, to be free during the fit. The most likely model is plotted in Figure 6 and a zoom in on the RM effect in Figure 7, showing the data slightly favor an aligned geometry. However, the median value and 68% confidence interval ($\lambda = 14^{+100}_{-64}$) show this constraint is extremely weak. In reality, the posterior for λ is bimodal with peaks at -30° and 120° , has a non-negligible probability everywhere, and is strongly influenced by the $v \sin I_*$ prior. In fact, the distribution of likely values is not far from uniform which would have a 68% confidence interval of 0 ± 123 degrees. Therefore, we consider λ to be essentially unconstrained. Note that in our quoted (median) values for angles, we first center the distribution about the mode to prevent boundary effects from skewing the inferred value to the middle of the arbitrary range.

Finally, we fit a separate transit time, baseline flux, and detrend with airmass to each of the 19 transits during the global fit, a separate zero point for each of the 4 RV data sets, and a slope to detect an RV trend, for a total of 75 free parameters (73 for the circular fit).

3.4. Transit Timing Variations

Great care was taken to translate each of our timestamps to a common system, BJD_{TDB} (Eastman et al. 2010). All observers report JD_{UTC} at mid exposure and

the translation to BJD_{TDB} is done uniformly for all observations prior to the fit. In addition, we have double checked the values quoted directly from an example image header for each observer. During the global fit, the transit time for each of the 19 transits were allowed to vary freely, as shown in Figure 11 and summarized in Table 7. While most epochs were consistent with a linear ephemeris,

$$T_0 = 2456193.29157 \pm 0.00021, P = 2.9895936 \pm 0.0000048, \quad (1)$$

there are a few large outliers. However, given the TTV results for Hot Jupiters from the Kepler mission (Steffen et al. 2012), the heterogeneity of our clocks, observatories, and observing procedures, and the potential for atmospheric and astrophysical sources of red noise to skew our transit times by amounts larger than our naive error estimates imply (Carter & Winn 2009), we do not view these outliers as significant. In particular, our experience with KELT-3b (Pepper et al. 2013), where we observed the same epoch with 3 different telescopes and found that the observation from FLWO differed by 5-sigma (7 minutes) from the other two with no discernible cause has led us to be skeptical of all ground-based TTV detections. Curiously, the two most significant outliers are also from FLWO, possibly pointing to a problem with the stability of its observatory clock (at the 5-10 minute level). We have set up monitoring of this clock and are watching it closely both for drifts and short-term glitches. While we feel our skepticism of these nominally significant TTVs is warranted, the recent results for WASP-47b (Becker et al. 2015) is a counter-example to the observation that Hot Jupiters tend not to have companions, so these outliers may be worth additional follow-up with a more homogeneous setup.

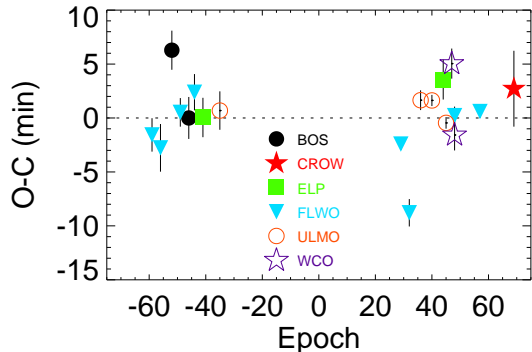


FIG. 11.— The transit times of the 19 transits of KELT-4Ab with the best-fit linear ephemeris ($T_0 = 2456193.29157 \pm 0.00021$, $P = 2.9895936 \pm 0.0000048$) subtracted.

4. FALSE POSITIVE REJECTION

False positives due to background eclipsing binaries are common in transit surveys. As such, all KELT candidates are subject to a rigorous set of tests to eliminate such scenarios. While our AO results show that our survey data and followup photometry were diluted by a companion binary system, KELT-4A was resolved in all of

TABLE 5
 MEDIAN VALUES AND 68% CONFIDENCE INTERVAL FOR THE LIMB
 DARKENING PARAMETERS FOR KELT-4A

Parameter	Units	Eccentric	Circular
$u_{1,CoRoT} \dots$	Linear Limb-darkening ...	0.3216	0.3217
$u_{2,CoRoT} \dots$	Quadratic Limb-darkening	0.2970	0.2969
$u_{1,g'} \dots \dots$	Linear Limb-darkening ...	0.472	0.472
$u_{2,g'} \dots \dots$	Quadratic Limb-darkening	0.2697	0.2697
$u_{1,r'} \dots \dots$	Linear Limb-darkening ...	0.3126	0.3127
$u_{2,r'} \dots \dots$	Quadratic Limb-darkening	0.3144	0.3143
$u_{1,i'} \dots \dots$	Linear Limb-darkening ...	0.2395	0.2396
$u_{2,i'} \dots \dots$	Quadratic Limb-darkening	0.3045	0.3044
$u_{1,I} \dots \dots$	Linear Limb-darkening ...	0.2216	0.2217
$u_{2,I} \dots \dots$	Quadratic Limb-darkening	0.3022	0.3022
$u_{1,z'} \dots \dots$	Linear Limb-darkening ...	0.1892	0.1893
$u_{2,z'} \dots \dots$	Quadratic Limb-darkening	0.2949	0.2948

the radial velocity observations used for analysis, which shows a clear signal of a planet. In addition, there was no evidence of any other background stars in the area (see §2.5). We also observed transits of KELT-4Ab in six different filters to check for a wavelength-dependent transit depth indicative of a blend, but all transit depths in all bands were consistent with one another after accounting for the blend with the nearby companion.

5. INSOLATION EVOLUTION

Because KELT-4Ab is inflated, it is interesting to investigate its irradiation history, as described in Pepper et al. (2013), as an empirical probe into the timescale of inflation mechanisms (Assef et al. 2009; Spiegel & Madhusudhan 2012). Our results are shown in Figure 12. Similar to KELT-3b, the incident flux has always been above the inflation irradiation threshold identified by Demory & Seager (2011), regardless of our assumptions about the tidal Q factor. Similar to KELT-8b, it is likely spiraling into its host star with all reasonable values of the tidal Q factor (Fulton et al. 2015).

For this model, we matched the current conditions at the age of KELT-4A. However, we note that instead of using the YY stellar models as in the rest of the analysis, we used the YREC models (Siess et al. 2000; Demarque et al. 2008) here. As a result, we could not precisely match the stellar parameters used elsewhere in the modeling, but they were well within the quoted uncertainties.

6. DISCUSSION

The large separation of the planet host from the tight binary makes this system qualitatively similar to KELT-2Ab (Beatty et al. 2012). As such, we expect the Kozai mechanism (Kozai 1962; Lidov 1962) to influence the migration of KELT-4Ab as well, and therefore the KELT-4Ab system to be misaligned. With an expected RM amplitude of 50 m s^{-1} , this would be easy to detect, though complicated by its near-integer day period and nearby companion. It is well-positioned for RM observations at Keck in 2016. Like KELT-2A, the effective temperature of KELT-4A ($6206 \pm 75 \text{ K}$) is near the dividing line between cool aligned stars and hot misaligned stars noted by Winn et al. (2010).

Interestingly, relative periods discussed in §2.5 set a Kozai-Lidov (KL) timescale of 540,000 years for the

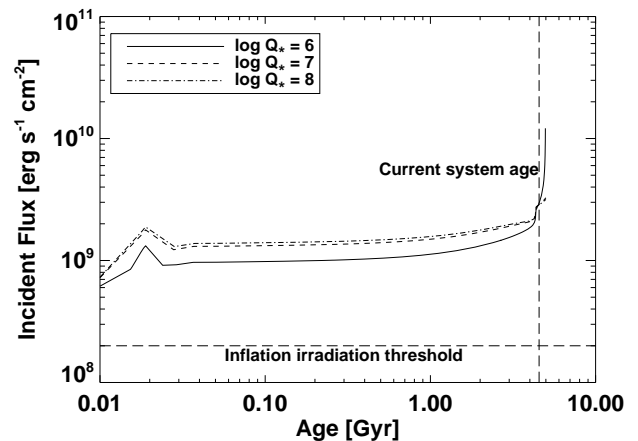


FIG. 12.— Change in incident flux for KELT-4Ab, with different test values for Q_* for KELT-4A. In all cases the planet has always received more than enough flux from its host to keep the planet irradiated beyond the insolation threshold of $2 \times 10^8 \text{ erg s}^{-1} \text{ cm}^{-2}$ identified by Demory & Seager (2011).

KELT-4BC stellar binary (Pejcha et al. 2013). This is relatively short, so we may expect to find that BC is currently undergoing Kozai-Lidov cycles and therefore be highly eccentric. Its relatively short period makes this an excellent candidate for continued follow-up effort, though its current separation is right at the K-band diffraction limit for Keck (25.5 mas).

The planetary binary has a Kozai-Lidov timescale of 1.6 Gyr. This is well below the age of the system, but assuming KELT-4Ab formed beyond the snow line ($\sim 5 \text{ AU}$), its period would have been longer and therefore its Kozai-Lidov timescale shorter. This suggests Kozai is a plausible migration mechanism.

If KELT-4Ab formed past the ice line at a few AU and migrated to its present location via Kozai-Lidov oscillations and tidal friction (as in, e.g., Wu & Murray 2003; Fabrycky & Tremaine 2007), this would place constraints on the orbital parameters of the system as it existed shortly after formation. In particular, for Kozai-Lidov oscillations to be strong enough to drive the planet from $\sim 5 \text{ AU}$ to 0.04 AU either the initial inclination of the outer orbit relative to the planet must have been

TABLE 6
 MEDIAN VALUES AND 68% CONFIDENCE INTERVAL FOR KELT-4AB

Parameter	Units	Eccentric	Circular
Stellar Parameters:			
M_*	Mass (M_\odot)	$1.204^{+0.072}_{-0.063}$	$1.201^{+0.067}_{-0.061}$
R_*	Radius (R_\odot)	$1.610^{+0.078}_{-0.068}$	$1.603^{+0.039}_{-0.038}$
L_*	Luminosity (L_\odot)	$3.46^{+0.43}_{-0.38}$	$3.43^{+0.28}_{-0.27}$
ρ_*	Density (cgs)	0.407 ± 0.044	$0.411^{+0.018}_{-0.017}$
Age	Age (Gyr)	$4.38^{+0.81}_{-0.88}$	$4.44^{+0.78}_{-0.89}$
$\log g_*$	Surface gravity (cgs)	$4.105^{+0.029}_{-0.032}$	4.108 ± 0.014
T_{eff}	Effective temperature (K)	6207^{+75}_{-76}	6206 ± 75
[Fe/H]	Metallicity	$-0.116^{+0.067}_{-0.071}$	$-0.116^{+0.065}_{-0.069}$
$v \sin I_*$	Rotational velocity (m/s)	6000 ± 1200	6000 ± 1200
λ	Spin-orbit alignment (degrees)	30^{+85}_{-74}	14^{+100}_{-64}
d	Distance (pc)	211^{+13}_{-12}	210.7 ± 9.0
Planetary Parameters:			
e	Eccentricity	$0.030^{+0.036}_{-0.021}$	—
ω_*	Argument of periastron (degrees)	60^{+110}_{-120}	—
P	Period (days)	2.9895933 ± 0.0000049	2.9895932 ± 0.0000049
a	Semi-major axis (AU)	$0.04321^{+0.00085}_{-0.00077}$	$0.04317^{+0.00079}_{-0.00074}$
M_P	Mass (M_J)	$0.878^{+0.070}_{-0.067}$	$0.902^{+0.060}_{-0.059}$
R_P	Radius (R_J)	$1.706^{+0.085}_{-0.076}$	$1.699^{+0.046}_{-0.045}$
ρ_P	Density (cgs)	$0.219^{+0.031}_{-0.029}$	$0.228^{+0.019}_{-0.018}$
$\log g_P$	Surface gravity	$2.873^{+0.042}_{-0.045}$	$2.889^{+0.029}_{-0.030}$
T_{eq}	Equilibrium temperature (K)	1827^{+44}_{-42}	1823 ± 27
Θ	Safronov number	$0.0368^{+0.0030}_{-0.0029}$	0.0381 ± 0.0024
$\langle F \rangle$	Incident flux ($10^9 \text{ erg s}^{-1} \text{ cm}^{-2}$)	$2.53^{+0.25}_{-0.23}$	2.51 ± 0.15
RV Parameters:			
T_C	Time of inferior conjunction (BJD_{TDB})	$2456190.30201 \pm 0.00022$	$2456190.30201 \pm 0.00022$
T_P	Time of periastron (BJD_{TDB})	$2456190.09^{+0.85}_{-0.97}$	—
K	RV semi-amplitude (m/s)	108.6 ± 7.4	$111.8^{+6.3}_{-6.4}$
K_R	RM amplitude (m/s)	72 ± 14	71 ± 14
$M_P \sin i$	Minimum mass (M_J)	$0.871^{+0.069}_{-0.066}$	$0.896^{+0.060}_{-0.058}$
M_P/M_*	Mass ratio	0.000695 ± 0.000049	0.000717 ± 0.000042
u	RM linear limb darkening	$0.6018^{+0.0078}_{-0.0068}$	$0.6018^{+0.0077}_{-0.0067}$
γ_{EXPERT}	m/s	317 ± 23	317 ± 16
γ_{FIES}	m/s	-98 ± 13	-99 ± 12
γ_{HIRES}	m/s	15.7 ± 7.4	15.9 ± 6.7
γ_{TRES}	m/s	-11 ± 15	-10 ± 13
$\dot{\gamma}$	RV slope (m/s/day)	-0.014 ± 0.044	$-0.013^{+0.040}_{-0.041}$
$e \cos \omega_*$	$0.004^{+0.025}_{-0.017}$	—
$e \sin \omega_*$	$0.002^{+0.039}_{-0.029}$	—
$f(m_1, m_2)$	Mass function (M_J)	$0.000000414^{+0.000000091}_{-0.000000079}$	$0.000000454^{+0.000000081}_{-0.000000073}$
σ_{EXPERT}	Error scaling for EXPERT	2.00	1.37
σ_{FIES}	Error scaling for FIES	1.00	1.00
σ_{HIRES}	Error scaling for HIRES	7.48	6.85
σ_{TRES}	Error scaling for TRES	2.32	2.09
Primary Transit Parameters:			
R_P/R_*	Radius of the planet in stellar radii	$0.10892^{+0.00054}_{-0.00055}$	0.10893 ± 0.00054
a/R_*	Semi-major axis in stellar radii	$5.77^{+0.20}_{-0.22}$	$5.792^{+0.086}_{-0.082}$
i	Inclination (degrees)	$83.11^{+0.48}_{-0.57}$	$83.16^{+0.22}_{-0.21}$
b	Impact parameter	$0.689^{+0.011}_{-0.012}$	$0.689^{+0.011}_{-0.012}$
δ	Transit depth	0.01186 ± 0.00012	0.01187 ± 0.00012
T_{FWHM}	FWHM duration (days)	0.11893 ± 0.00045	0.11892 ± 0.00044
τ	Ingress/egress duration (days)	$0.02535^{+0.00090}_{-0.00089}$	$0.02536^{+0.00089}_{-0.00088}$
T_{14}	Total duration (days)	$0.14428^{+0.00084}_{-0.00083}$	$0.14428^{+0.00084}_{-0.00083}$
P_T	A priori non-grazing transit probability	$0.1548^{+0.012}_{-0.0092}$	0.1539 ± 0.0022
$P_{T,G}$	A priori transit probability	$0.193^{+0.015}_{-0.011}$	$0.1915^{+0.0028}_{-0.0029}$
Secondary Eclipse Parameters:			
T_S	Time of eclipse (BJD_{TDB})	$2456188.815^{+0.047}_{-0.032}$	$2456188.80721 \pm 0.00022$
b_S	Impact parameter	$0.693^{+0.055}_{-0.043}$	—
$T_{S,\text{FWHM}}$	FWHM duration (days)	$0.11840^{+0.00073}_{-0.00027}$	—
τ_S	Ingress/egress duration (days)	$0.0256^{+0.0046}_{-0.0029}$	—
$T_{S,14}$	Total duration (days)	$0.1445^{+0.0027}_{-0.0038}$	—
P_S	A priori non-grazing eclipse probability	0.1540 ± 0.0022	—
$P_{S,G}$	A priori eclipse probability	0.1917 ± 0.0029	—

TABLE 7
 MEDIAN VALUES AND 68% CONFIDENCE INTERVAL FOR THE TRANSIT TIMES OF ALL 19 FOLLOW-UP LIGHT CURVES OF KELT-4AB FROM THE GLOBAL CIRCULAR FIT, ALONG WITH RESIDUALS FROM THE BEST-FIT LINEAR EPHEMERIS: $T_{C,N}(\text{BJD}_{\text{TDB}}) = 2456193.29157 \pm 0.00021 + N(2.9895936 \pm 0.0000048)$

Parameter	UT Date	Telescope	Filter	Epoch	T_C (BJD _{TDB})	O-C (sec)	O-C (σ_{T_C})
$T_{C,0}$	2012-03-30	FLWO	<i>i</i>	-59	2456016.9045 ± 0.0011	-94.08	-1.01
$T_{C,1}$	2012-04-08	FLWO	<i>g</i>	-56	2456025.8724 ± 0.0015	-166.03	-1.25
$T_{C,2}$	2012-04-20	BOS	<i>i</i>	-52	2456037.8371 ± 0.0013	377.05	3.46
$T_{C,3}$	2012-04-29	FLWO	<i>z</i>	-49	$2456046.80185 \pm 0.00092$	31.30	0.39
$T_{C,4}$	2012-05-08	BOS	<i>g</i>	-46	$2456055.7703^{+0.0014}_{-0.0013}$	0.14	0.00
$T_{C,5}$	2012-05-14	FLWO	<i>g</i>	-44	2456061.7511 ± 0.0012	143.37	1.42
$T_{C,6}$	2012-05-23	ELP	<i>g</i>	-41	2456070.7183 ± 0.0013	2.65	0.02
$T_{C,7}$	2012-06-10	ULMO	<i>r</i>	-35	2456088.6563 ± 0.0012	41.23	0.39
$T_{C,8}$	2012-12-18	FLWO	<i>i</i>	29	$2456279.98810 \pm 0.00038$	-145.14	-4.44
$T_{C,9}$	2012-12-27	FLWO	<i>i</i>	32	$2456288.95246^{+0.00087}_{-0.00089}$	-527.01	-6.92
$T_{C,10}$	2013-01-08	ULMO	<i>g</i>	36	$2456300.91808^{+0.00064}_{-0.00063}$	98.93	1.80
$T_{C,11}$	2013-01-20	ULMO	<i>g</i>	40	$2456312.87644 \pm 0.00036$	97.52	3.14
$T_{C,12}$	2013-02-01	ELP	<i>z</i>	44	$2456324.8362^{+0.0012}_{-0.0013}$	213.79	1.93
$T_{C,13}$	2013-02-04	ULMO	<i>g</i>	45	$2456327.82297 \pm 0.00037$	-27.14	-0.85
$T_{C,14}$	2013-02-10	WCO	<i>CBB</i>	47	$2456333.80597^{+0.00096}_{-0.00098}$	302.63	3.61
$T_{C,15}$	2013-02-13	WCO	<i>CBB</i>	48	$2456336.79097^{+0.0010}_{-0.00099}$	-94.51	-1.10
$T_{C,16}$	2013-02-13	FLWO	<i>z</i>	48	$2456336.79221^{+0.00057}_{-0.00058}$	13.23	0.26
$T_{C,17}$	2013-03-12	FLWO	<i>i</i>	57	$2456363.69882 \pm 0.00041$	35.76	1.01
$T_{C,18}$	2013-04-17	CROW	<i>I</i>	69	$2456399.5754^{+0.0025}_{-0.0024}$	162.86	0.77

close to 90° , or the eccentricity of the outer orbit must have been large, or both. We quantify these constraints by using the *kozai* Python package (Antognini 2015) to evolve a set of hierarchical triples in the secular approximation with the observed orbital parameters, but varying the outer eccentricity and the mutual inclination between the planetary orbit and the outer orbit. Although the KELT-4 system contains four bodies, we take the KELT-4BC system to be a point mass of $1.3 M_\odot$. Combinations of inclination and outer eccentricity that can drive strong enough Kozai-Lidov oscillations to bring the planet to within 0.02 AU^{29} of the star are shown in the unshaded region of Figure 13. Since the distribution of $\cos i$ between the planetary orbit and the outer orbit is expected to be uniform and the eccentricity distribution of wide binaries is also observed to be approximately uniform, equal areas of the right panel of Figure 13 can be interpreted as equal probabilities. Although we did not include relativistic precession in these calculations, we compared the precession timescale to the period of the KL oscillations and found that the precession timescale was much longer (at least a factor of 10) in all cases in which the KL oscillations are strong enough to drive KELT-4Ab to its present location.

While there are several planets in binary stellar systems, there are only a few transiting planets known in hierarchical triples. These systems may have had a richer dynamical history than the more commonly found planets in binary systems. Pejcha et al. (2013) and Hamers et al. (2015) have found that in quadruple systems the presence of the additional body can, in some cases, lead to resonant interactions between the Kozai-Lidov oscillations that occur in the inner binaries, thereby producing stronger eccentricity oscillations than in hierarchical triples with similar orbital parameters. Due to the small mass of KELT-4Ab it would not have had any strong dynamical influence on KELT-4BC, but the binarity of KELT-4BC may have influenced the dynamical evolution of KELT-4Ab. The discovery of systems like KELT-4 highlights the need for further study of the dynamics of quadruple systems.

High-resolution imaging and RV monitoring of both KELT-4A and KELT-4BC is likely to constrain the orbit of the twins relatively well in a short time. Their inclination and eccentricity is likely to provide insight into the formation and dynamical evolution of the system. The very long period of KELT-4BC around KELT-4A makes characterizing the orbit of the KELT-4BC binary around the KELT-4A primary more challenging, but continued monitoring may be able to exclude certain inclinations or eccentricities.

We expect, in the three years since the original AO observations, motions of $\sim 37 \text{ mas}$ between KELT-4B and KELT-4C, which should be easily visible. Between KELT-4A and KELT-4BC, the motions are expected to be $\sim 10 \text{ mas}$, which should also be marginally detectable with additional Keck observations. *Gaia* (Perryman et al. 2001) will provide new absolute astrometric measurements on KELT-4A to $\sim 7 \mu\text{as}$ and an unresolved position of KELT-4BC to $\sim 25 \mu\text{as}$. With

$\sim 25 \mu\text{as}$ accuracy, *Gaia* could see significant motion of KELT-4BC in ~ 3 days. *Gaia* will also provide a precise distance which will allow us to infer the radius of the primary, thereby distinguishing between the marginally inconsistent stellar parameters.

The maximum RV semi-amplitude of KELT-4A induced by the KELT-BC system, (i.e., assuming an edge-on orbit), would be 1.3 km s^{-1} or $0.002 \text{ m s}^{-1} \text{ day}^{-1}$. Since a separate zero point is fit for each data set, we are not sensitive to secular drifts that span the entire data set. We allowed the slope to be free during the fit, but the uncertainty is a factor of 20 larger than the expected signal. Still, it is not unrealistic to expect to detect a drift with long-term monitoring. The KELT-4BC system would have a maximum semi-amplitude of 5.3 km s^{-1} or about $2 \text{ m s}^{-1} \text{ day}^{-1}$, which is easily detectable, though its $V = 13$ magnitude and $1.5''$ separation from the primary star make it a challenging target.

This inflated hot Jupiter, while not unique (e.g., HAT-P-39b, HAT-P-40b, HAT-P-41b (Hartman et al. 2012)), like all KELT planets, is among the brightest and therefore easiest to follow up as a result of our survey design (see Figure 14). In particular, high-resolution imaging capable of resolving the stellar binary (42 mas) would help constrain the orbit of KELT-4BC, and may help create a more robust migration history of the entire system.

We thank Geoff Marcy for use of his Keck/HIRES time and doing observations. We extend special thanks to those of Hawai’ian ancestry on whose sacred mountain of Mauna Kea we are privileged to be guests. Without their generous hospitality, the Keck observations presented herein would not have been possible. Early work on KELT-North was supported by NASA Grant NNG04G070G. Work by B.S.G., J.D.E., and T.G.B. was partially supported by NSF CAREER Grant AST-1056524. K.A.C. was supported by a NASA Kentucky Space Grant Consortium Graduate Fellowship. J.A.P. and K.G.S. acknowledge support from the Vanderbilt Office of the Provost through the Vanderbilt Initiative in Data-intensive Astrophysics. K.G.S. and L.H. acknowledge the support of the National Science Foundation through PAARE grant AST-0849736 and AAG grant AST-1009810. The TRES and KeplerCam observations were obtained with partial support from the Kepler Mission through NASA Cooperative Agreement NNX11AB99A with the Smithsonian Astrophysical Observatory, D.W.L. PI. J. M. O. A. is supported in part by NSF Award #1313252. J.G., B.M., and J.W. acknowledge support from NSF AST-0705139 and the University of Florida for the development of the EXPERT instrument and observations. This material is based upon work supported by the National Science Foundation Graduate Research Fellowship under grant No. 2014184874. Any opinion, findings, and conclusions or recommendations expressed in this material are those of the authors(s) and do not necessarily reflect the views of the National Science Foundation.

The Byrne Observatory at Sedgwick (BOS) is operated by the Las Cumbres Observatory Global Telescope Network and is located at the Sedgwick Reserve, a part of the University of California Natural Reserve System.

²⁹ the planet circularizes at twice the initial periastron distance due to conservation of angular momentum (Fabrycky & Tremaine 2007)

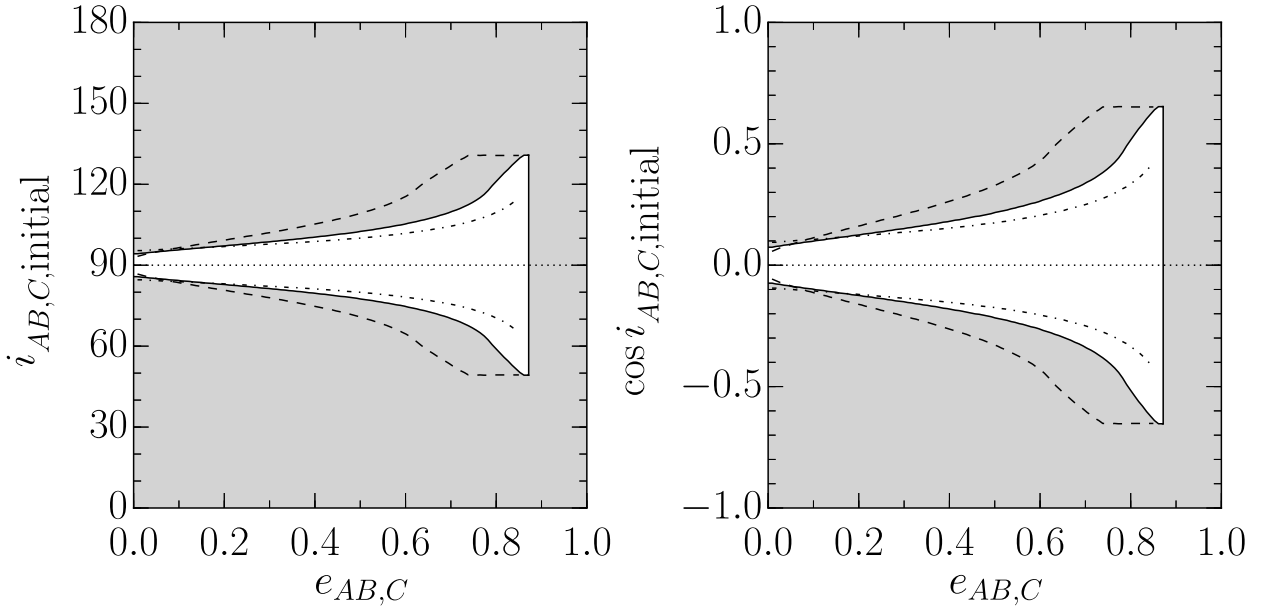


FIG. 13.— Ranges of initial inclination and outer eccentricity for which Kozai-Lidov oscillations can drive KELT-4Ab to its present semi-major axis, starting from a semi-major axis of 3 AU (dot-dashed line), 5 AU (solid line), and 10 AU (dashed line). The upper limit on the eccentricity is due to the requirement that the system be dynamically stable. We show in the right panel the same constraints, but with the cosine of the initial inclination rather than the inclination itself. Because $\cos i$ is expected to be uniformly distributed in hierarchical triples and the distribution of eccentricities of wide binaries is also observed to be approximately uniform, equal areas of this plot may be interpreted as equal probabilities.

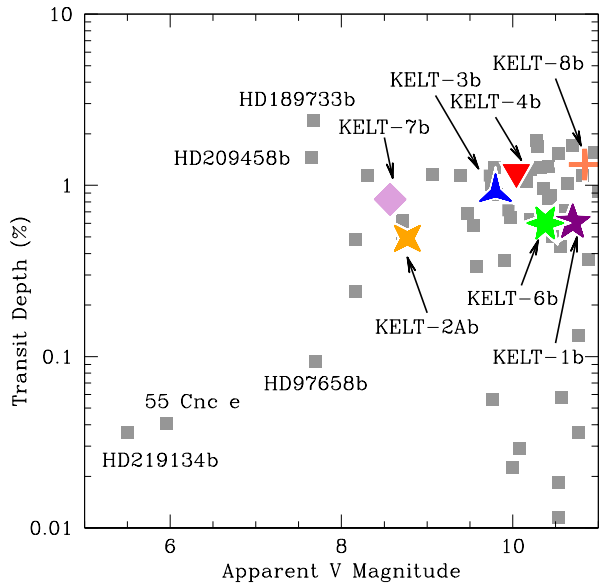


FIG. 14.— Transit depth as a function of the apparent V magnitude of the host star for a sample of transiting systems. KELT-4Ab is shown as the red triangle. All else being equal, objects in the top left provide the best targets for follow-up. The other discoveries from the KELT survey are also shown.

This work makes use of observations from the LCOGT network.

This work has made use of NASA’s Astrophysics Data System, the Extrasolar Planet Encyclopedia at exoplanet.eu (Schneider et al. 2011), the SIMBAD database operated at CDS, Strasbourg, France, and the VizieR catalogue access tool, CDS, Strasbourg, France (Ochsenbein et al. 2000). Certain calculations in this paper were carried out on the Ruby cluster operated by the Ohio Supercomputer Center (Center 2015).

This publication makes use of data products from the Wide-field Infrared Survey Explorer, which is a joint project of the University of California, Los Angeles, and the Jet Propulsion Laboratory/California Institute of Technology, funded by the National Aeronautics and Space Administration.

This publication makes use of data products from the Two Micron All Sky Survey, which is a joint project of the University of Massachusetts and the Infrared Processing and Analysis Center/California Institute of Technology, funded by the National Aeronautics and Space Administration and the National Science Foundation.

This paper makes use of data from the first public release of the WASP data (Butters et al. 2010) as provided by the WASP consortium and services at the NASA Exoplanet Archive (Akeson et al. 2013), which is operated by the California Institute of Technology, under contract with the National Aeronautics and Space Administration under the Exoplanet Exploration Program, the Exoplanet Orbit Database and the Exoplanet Data Explorer at exoplanets.org (Wright et al. 2011).

REFERENCES

Adams, F. C., & Laughlin, G. 2006, *ApJ*, 649, 1004
Akeson, R. L., et al. 2013, *PASP*, 125, 989

Alonso, R., et al. 2004, *ApJ*, 613, L153
Antognini, J. M. O. 2015, *MNRAS*, 452, 3610

- Argue, A. N., Bunclark, P. S., Irwin, M. J., Lampens, P., Sinachopoulos, D., & Wayman, P. A. 1992, *MNRAS*, 259, 563
- Assef, R. J., Gaudi, B. S., & Stanek, K. Z. 2009, *ApJ*, 701, 1616
- Baglin, A., et al. 2006, in *COSPAR, Plenary Meeting, Vol. 36, 36th COSPAR Scientific Assembly*, 3749+
- Bakos, G. Á., Lázár, J., Papp, I., Sári, P., & Green, E. M. 2002, *PASP*, 114, 974
- Beatty, T. G., & Gaudi, B. S. 2008, *ApJ*, 686, 1302
- Beatty, T. G., et al. 2012, *ApJ*, 756, L39
- Bechter, E. B., et al. 2014, *ApJ*, 788, 2
- Becker, J. C., Vanderburg, A., Adams, F. C., Rappaport, S. A., & Schwengel, H. M. 2015, *ArXiv e-prints*
- Bensby, T., Feltzing, S., & Lundström, I. 2003, *A&A*, 410, 527
- Brown, T. M., et al. 2013, *PASP*, 125, 1031
- Buchhave, L. A., et al. 2010, *ApJ*, 720, 1118
- . 2012, *Nature*, 486, 375
- . 2014, *Nature*, 509, 593
- Butters, O. W., et al. 2010, *A&A*, 520, L10
- Carter, J. A., & Winn, J. N. 2009, *ApJ*, 704, 51
- Center, O. S. 2015
- Charbonneau, D., Brown, T. M., Latham, D. W., & Mayor, M. 2000, *ApJ*, 529, L45
- Charbonneau, D., Brown, T. M., Noyes, R. W., & Gilliland, R. L. 2002, *ApJ*, 568, 377
- Charbonneau, D., et al. 2006, *ApJ*, 636, 445
- Chubak, C., Marcy, G., Fischer, D. A., Howard, A. W., Isaacson, H., Johnson, J. A., & Wright, J. T. 2012, *ArXiv e-prints*
- Claret, A., & Bloemen, S. 2011, *A&A*, 529, A75+
- Coşkunoglu, B., et al. 2011, *MNRAS*, 412, 1237
- Collier Cameron, A., et al. 2007, *MNRAS*, 375, 951
- Collins, K., & Kielkopf, J. 2013, *AstroImageJ: ImageJ for Astronomy, Astrophysics Source Code Library*
- Collins, K. A. 2015, *Electronic Theses and Dissertations, Paper 2104*
- Collins, K. A., et al. 2014, *AJ*, 147, 39
- Couteau, P. 1973, *A&AS*, 10, 273
- Cutri, R. M., & et al. 2012, *VizieR Online Data Catalog*, 2311, 0
- Cutri, R. M., et al. 2003, *VizieR Online Data Catalog*, 2246, 0
- Demarque, P., Guenther, D. B., Li, L. H., Mazumdar, A., & Straka, C. W. 2008, *Ap&SS*, 316, 31
- Demarque, P., Woo, J.-H., Kim, Y.-C., & Yi, S. K. 2004, *ApJS*, 155, 667
- Demory, B.-O., & Seager, S. 2011, *ApJS*, 197, 12
- Demory, B.-O., et al. 2009, *A&A*, 505, 205
- Djupvik, A. A., & Andersen, J. 2010, in *Highlights of Spanish Astrophysics V*, ed. J. M. Diego, L. J. Goicoechea, J. I. González-Serrano, & J. Gorgas, 211
- Dragomir, D., et al. 2013, *ApJ*, 772, L2
- Eastman, J., Gaudi, B. S., & Agol, E. 2013, *PASP*, 125, 83
- Eastman, J., Siverd, R., & Gaudi, B. S. 2010, *PASP*, 122, 935
- Fabrycius, C., Høg, E., Makarov, V. V., Mason, B. D., Wycoff, G. L., & Urban, S. E. 2002, *A&A*, 384, 180
- Fabrycky, D., & Tremaine, S. 2007, *ApJ*, 669, 1298
- Fűrész, G. 2008, *PhD Thesis, Univ. Szeged, Hungary*
- Flower, P. J. 1996, *ApJ*, 469, 355
- Fortney, J. J., Saumon, D., Marley, M. S., Lodders, K., & Freedman, R. S. 2006, *ApJ*, 642, 495
- Fulton, B. J., et al. 2015, *ApJ*, 810, 30
- Gaudi, B. S., & Winn, J. N. 2007, *ApJ*, 655, 550
- Ge, J., et al. 2010, in *Society of Photo-Optical Instrumentation Engineers (SPIE) Conference Series, Vol. 7735, Society of Photo-Optical Instrumentation Engineers (SPIE) Conference Series*
- Guillot, T. 2005, *Annual Review of Earth and Planetary Sciences*, 33, 493
- Hamers, A. S., Perets, H. B., Antonini, F., & Portegies Zwart, S. F. 2015, *MNRAS*, 449, 4221
- Hartman, J. D., et al. 2012, *AJ*, 144, 139
- Hauschildt, P. H., Allard, F., & Baron, E. 1999, *ApJ*, 512, 377
- Henden, A. A., Levine, S. E., Terrell, D., Smith, T. C., & Welch, D. 2012, *Journal of the American Association of Variable Star Observers (JAAVSO)*, 40, 430
- Henry, G. W., Marcy, G. W., Butler, R. P., & Vogt, S. S. 2000, *ApJ*, 529, L41
- Høg, E., et al. 2000, *A&A*, 355, L27
- Howard, A. W., et al. 2010, *ApJ*, 721, 1467
- Kovács, G., Bakos, G., & Noyes, R. W. 2005, *MNRAS*, 356, 557
- Kovács, G., Zucker, S., & Mazeh, T. 2002, *A&A*, 391, 369
- Kozai, Y. 1962, *AJ*, 67, 591
- Lidov, M. L. 1962, *Planet. Space Sci.*, 9, 719
- Martin, D. C., et al. 2005, *ApJ*, 619, L1
- Mason, B. D., Wycoff, G. L., Hartkopf, W. I., Douglass, G. G., & Worley, C. E. 2001, *AJ*, 122, 3466
- Mayor, M., & Queloz, D. 1995, *Nature*, 378, 355
- McCullough, P. R., Stys, J. E., Valenti, J. A., Fleming, S. W., James, K. A., & Heasley, J. N. 2005, *PASP*, 117, 783
- Neveu-VanMalle, M., et al. 2014, *A&A*, 572, A49
- Ochsenbein, F., Bauer, P., & Marcout, J. 2000, *A&AS*, 143, 23
- Ohta, Y., Taruya, A., & Suto, Y. 2005, *ApJ*, 622, 1118
- Pejcha, O., Antognini, J. M., Shappee, B. J., & Thompson, T. A. 2013, *ArXiv e-prints*
- Pepper, J., et al. 2007, *PASP*, 119, 923
- . 2013, *ApJ*, 773, 64
- Perryman, M. A. C., et al. 1997, *A&A*, 323, L49
- . 2001, *A&A*, 369, 339
- Queloz, D., Eggenberger, A., Mayor, M., Perrier, C., Beuzit, J. L., Naef, D., Sivan, J. P., & Udry, S. 2000, *A&A*, 359, L13
- Ricker, G. R., et al. 2010, in *Bulletin of the American Astronomical Society, Vol. 42, American Astronomical Society Meeting Abstracts 215*, 450.06
- Sato, B., et al. 2005, *ApJ*, 633, 465
- Schlegel, D. J., Finkbeiner, D. P., & Davis, M. 1998, *ApJ*, 500, 525
- Schneider, J., Dedieu, C., Le Sidaner, P., Savalle, R., & Zolotukhin, I. 2011, *A&A*, 532, A79
- Seager, S., & Mallén-Ornelas, G. 2003, *ApJ*, 585, 1038
- Siess, L., Dufour, E., & Forestini, M. 2000, *A&A*, 358, 593
- Siverd, R. J., et al. 2012, *ArXiv e-prints*
- Skrutskie, M. F., et al. 2006, *AJ*, 131, 1163
- Smalley, B., et al. 2012, *A&A*, 547, A61
- Spiegel, D. S., & Madhusudhan, N. 2012, *ApJ*, 756, 132
- Steffen, J. H., et al. 2012, *ApJ*, 756, 186
- Torres, G., Andersen, J., & Giménez, A. 2010, *A&A Rev.*, 18, 67
- Torres, G., Fischer, D. A., Sozzetti, A., Buchhave, L. A., Winn, J. N., Holman, M. J., & Carter, J. A. 2012, *ApJ*, 757, 161
- TriAUD, A. H. M. J., et al. 2010, *A&A*, 524, A25
- van Leeuwen, F. 2007, *A&A*, 474, 653
- Vidal-Madjar, A., Lecavelier des Etangs, A., Désert, J., Ballester, G. E., Ferlet, R., Hébrard, G., & Mayor, M. 2003, *Nature*, 422, 143
- Vogt, S. S., et al. 1994, in , 362
- Wang, Sharon, X., et al. 2012, *ApJ*, 761, 46
- Winn, J. N. 2010, *Exoplanet Transits and Occultations*, ed. Seager, S., 55–77
- Winn, J. N., Fabrycky, D., Albrecht, S., & Johnson, J. A. 2010, *ApJ*, 718, L145
- Winn, J. N., et al. 2005, *ApJ*, 631, 1215
- Wright, E. L., et al. 2010, *AJ*, 140, 1868
- Wright, J. T., et al. 2011, *PASP*, 123, 412
- Wu, Y., & Murray, N. 2003, *ApJ*, 589, 605
- Yelda, S., Lu, J. R., Ghez, A. M., Clarkson, W., Anderson, J., Do, T., & Matthews, K. 2010, *ApJ*, 725, 331
- Yi, S., Demarque, P., Kim, Y.-C., Lee, Y.-W., Ree, C. H., Lejeune, T., & Barnes, S. 2001, *ApJS*, 136, 417

